Bulletin of the Seismological Society of America, Vol. 103, No. 6, pp. 3044–3056, December 2013, doi: 10.1785/0120120312

Stochastic Model for Earthquake Ground Motion Using Wavelet Packets

by Yoshifumi Yamamoto and Jack W. Baker

Abstract For performance-based design, nonlinear dynamic structural analysis using various types of input ground motions is required. Stochastic (simulated) ground motions are sometimes useful as input motions, because their properties can be varied systematically to study the impact of ground-motion properties on structural response, and producing large numbers of ground motions is simple. This paper describes an approach by which the wavelet packet transform can be used to characterize complex time-varying earthquake ground motions, and it illustrates the potential benefits of such an approach in a variety of earthquake engineering applications. A model is developed that requires 13 parameters to describe a given ground motion. These 13 parameters are then related to seismological variables such as earthquake magnitude, distance, and site condition, through regression analysis that captures trends in mean values, standard deviations, and correlations of these parameters observed in recorded strong ground motions from 25 past earthquakes. The resulting regression equations can then be used to predict ground motions for a future earthquake scenario. This model is analogous to widely used empirical ground-motion prediction equations (formerly called attenuation models) except that this model predicts entire time series rather than only response spectra. The ground motions produced using this predictive model are explored in detail, and have elastic response spectra, inelastic response spectra, durations, mean periods, and so forth, that are consistent in both mean and variability with existing published predictive models for those properties.

Introduction

Nonlinear dynamic structural analysis generally requires the use of large numbers of input ground motions in order to determine the performance of structures in terms of probability distributions of engineering demand parameters, which are used for performance-based design. However, the number of available recorded ground motions is limited and may not be sufficient for characterizing a particular analysis condition.

In order to obtain additional ground motions for a particular analysis condition, ground-motion scaling and spectral matching are widely used to adjust recorded ground motions and make them more representative of the target analysis condition. However, these approaches change the relationship between characteristics of recorded ground motions and their original physical conditions, so the results of these operations could have characteristics different from those of actual recorded ground motions (e.g., Luco and Bazzurro, 2007). An alternative approach is, therefore, to generate artificial earthquake ground motions whose characteristics are consistent with both the physical condition of interest and the characteristics of the actual recorded ground motions.

There are three general types of strong ground motion simulation techniques (Douglas and Aochi, 2008): physics-based simulations that generate ground motions by modeling fault rupture and resulting wave propagation (e.g., Pitarka *et al.*, 1998), stochastic simulations that are empirically calibrated approaches to directly simulate the recorded ground motions with target seismological and probabilistic characteristics including variability of ground motions (e.g., Rezaeian and Der Kiureghian, 2010, 2012), and hybrid simulations which combine the first two (e.g., Graves and Pitarka, 2010). We focus on the stochastic simulations in this paper. With stochastic simulations, it is difficult to consider physical phenomena such as surface waves, directivity, etc., explicitly because there are likely no parameters in the model to control these effects; stochastic simulations may be appealing in some cases, however, because stochastic simulations require fewer parameters and are computationally less expensive than physics-based and hybrid simulations.

Regarding stochastic simulations, there are a number of comprehensive literature reviews available (e.g., Shinozuka and Deodatis, 1988; Rezaeian, 2010). One of the important issues raised in these reviews is that of time and frequency nonstationarity, which describes the changing amplitudes of time series (temporal nonstationarity) and changing frequency characteristics (spectral nonstationarity) in time. It can affect the results of nonlinear dynamic structural analysis

(e.g., Conte, 1992; Spanos, Giaralis, and Politis, 2007), in part because the structure's behavior is also nonstationary as it is driven to nonlinear response and its resulting natural period increases (Papadimitrios, 1990).

Rezaeian (2010) places existing stochastic ground-motion models into four categories: (1) processes obtained by passing a white noise through a filter (e.g., Shinozuka and Sato, 1967; Alamilla *et al.*, 2001) with subsequent modulation in time for temporal nonstationarity; (2) processes obtained by passing a train of Poisson pulses through a linear filter (e.g., Cornell, 1964), these processes can generate ground motions with time and frequency nonstationarity using modulation in time (Lin, 1986); (3) autoregressive moving average (ARMA) models (e.g., Hoshiya and Hasgur, 1978; Sgobba *et al.*, 2011), Sgobba *et al.* (2011) proposed the model with parameters related to seismological information through regression analysis; and (4) various forms of spectral representation (e.g., Page, 1952; Priestley, 1965; Pousse *et al.*, 2006). These models use a short-time Fourier transform or wavelet transform to develop a time-frequency modulating function that matches a particular recorded ground motion. Also, Thráinsson and Kiremidjian (2002) use phase differences in the ground-motion components of various frequencies to generate ground motions with time-frequency nonstationarity. The model proposed in this paper characterizes the signal in the time and frequency domain using wavelet transforms, so it fits into the fourth category.

Various researchers have used the wavelet transform to characterize ground motions. Among them, Masuda and Sone (2002) and Spanos *et al.* (2007) generated artificial ground motions with specified time and frequency characteristics. Their implementations were limited, however, to produce simulations that reproduced properties of a "seed" ground motion that was used for calibration, rather than producing simulations for an arbitrary future earthquake scenario. Nakamura *et al.* (2008) proposed a model to generate artificial ground motions having a target response spectra using a linear combination of wavelet coefficients from a large number of recorded ground motions using the discrete wavelet transform (DWT). The time and frequency characteristics of the simulated motions are taken to match those of a reference recorded ground motion. Amiri *et al.* (2011) used the wavelet packet transform (WPT) to generate artificial ground motions compatible with a target pseudovelocity response spectrum and having time and frequency nonstationarity. Their model used a neural network to predict the amplitudes of wavelet packet coefficients. The simulations from this model are conditional on a target spectrum rather than seismological parameters, however, so it is difficult to generate ground motions that represent the full variability of potential future ground motions. Sasaki *et al.* (2003) proposed a model using the DWT to generate artificial ground motions with time and frequency nonstationarity, and attenuation models to predict their model parameters. However, the DWT has limited ability to control the time location of long-period energy, and the realism of variability in the simulated ground motions is not discussed.

In this paper, the WPT is employed in order to quantify the time and frequency characteristics of time series for stochastic ground-motion modeling. Among options for wavelet analysis, the continuous wavelet transform is difficult to use to reconstruct time series, due to the nonorthogonality of the wavelets at adjacent times and frequencies, and the DWT has low time-domain resolution at long periods, making it difficult to control long-period properties of the simulations. The WPT is the extended version of the DWT. The WPT allows much more flexibility in controlling resolution in the time and frequency domains, and its basis functions are orthogonal, which allows for easy reconstruction of time series by simulating wavelet packets. For these reasons, the WPT has been noted by several of the above-cited authors as an effective tool for producing nonstationary time series.

Another important feature of the proposed stochastic ground-motion model is the variability of simulated ground motions, as this affects the variability of structural responses (e.g., Rezaeian and Der Kiureghian, 2010, 2012). The proposed model requires 13 model parameters that are predicted via regression models. The regression model includes variability in predicted parameters, and this introduces appropriate variability into the properties of the simulated ground motions. The simulated ground motions from the proposed model are observed to have similar characteristics to existing ground-motion prediction equations (GMPEs) in terms of the median and variability of spectral acceleration (e.g., Boore and Atkinson, 2008), correlation of residuals (Baker and Jayaram, 2008), inelastic response spectra (Bozorgnia *et al.*, 2010), Arias intensity (Arias, 1970), mean period (Rathje *et al.*, 2004), and significant duration (Trifunac and Brady, 1976). The realism of the simulated motions with respect to so many parameters of engineering interest suggests that these simulations are appropriate for use in structural analysis or hazard analysis.

Stochastic Ground-Motion Model

Wavelet Packet Transform

We employ the WPT to decompose a ground-motion time series into wavelet packets in the time and frequency domain, and to reconstruct a time series from wavelet packets. The WPT is a modified version of the wavelet transform defined as follows:

$$c^i_{j,k} = \int_{-\infty}^{\infty} x(t)\psi^i_{j,k}(t)dt, \tag{1}$$

in which $x(t)$ is the time series, $c^i_{j,k}$ denotes the ith set of wavelet packet coefficients at the jth scale parameter and kth translation parameter, and $\psi^i_{j,k}(t)$ is the wavelet packet function. The parameter i indicates the location of the wavelet packet in the frequency axis, parameter j indicates the frequency resolution, and k indicates its location in the time

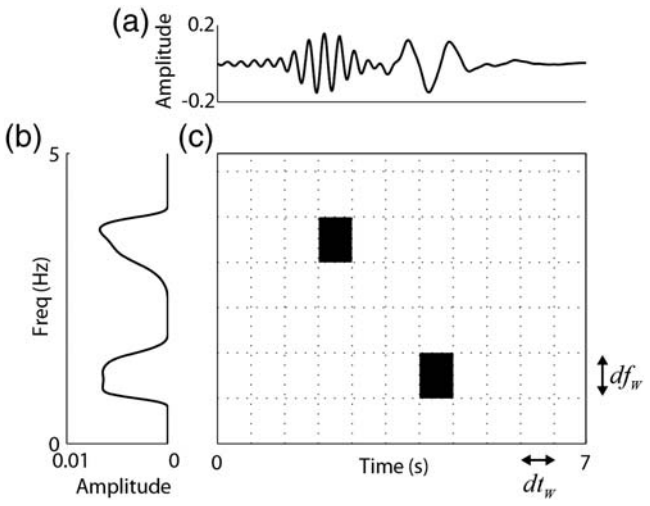

Figure 1. The relationship between the time, frequency, and wavelet domain. (a) Time series, (b) Fourier spectrum, and (c) wavelet packets. Black squares in (c) indicate nonzero wavelet packet coefficients at the corresponding time and frequency.

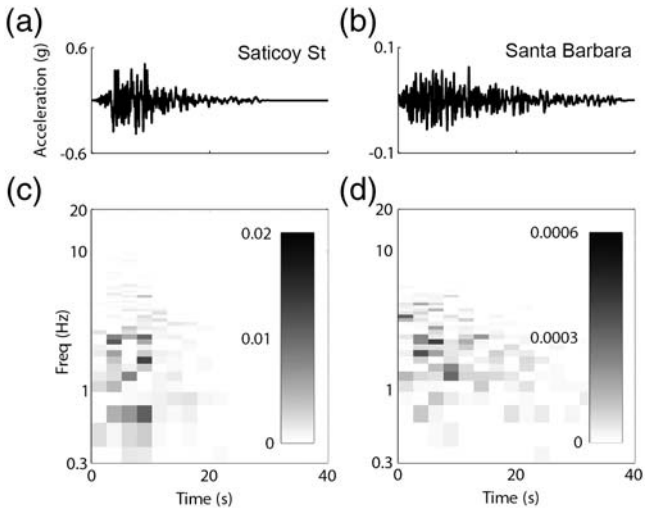

Figure 2. Wavelet packets for two example time series from the 1994 Northridge California earthquake. (a) Acceleration time series and (c) squared amplitudes of wavelet packet coefficients from the Saticoy Street recording, (b) acceleration time series, and (d) squared amplitudes of wavelet packet coefficients from the UCSB Goleta recording. The gray scales in (c) and (d) indicate the squared amplitudes of wavelet packet coefficients.

axis. Assuming $\psi^i_{j,k}(t)$ is localized on the time and frequency axes, the wavelet packets are related closely to the energy distribution of the time series in the time and frequency domain.

It is possible to reconstruct a time series from wavelet packets using the inverse WPT as follows:

$$x(t) = \sum_{i=1}^{2^j} \sum_{k=1}^{2^{N-j}} c^i_{j,k} \psi^i_{j,k}(t), \tag{2}$$

in which 2^N is the number of time steps in the time series. The number of wavelet packets required to describe a time series is thus equal to the number of time steps. There are a number of wavelet packet functions that can be used in these transforms. Here the wavelet packet function is computed from the finite-impulse response-based approximation of the Meyer wavelet (Meyer, 1986) because it is orthogonal and has good localization in both the time axis and the frequency axis. The relationship between the time, frequency, and the wavelet domain of time-series data is illustrated in Figure 1. The approximate time interval (dt_w) and frequency interval (df_w) between the centers of adjacent wavelet packets can be defined as follows:

$$dt_w = \frac{2^N dt}{2^{N-j}} = 2^j dt, \tag{3}$$

$$df_w = \frac{f_N}{2^j} = \frac{1}{2dt}\frac{1}{2^j}, \tag{4}$$

in which 2^N is the number of data in the time series, j is the scale parameter, dt is the time step of the time series, and f_N is the Nyquist frequency. In our model, $dt = 0.01$ s and $j = 8$, which leads to reasonable control of frequencies as low as 0.1 Hz, and wavelet packets in the lowest frequency level are controlled to ensure no residual velocities in simulated time series.

To illustrate the result of WPTs for ground motions, Figure 2 shows acceleration time series data of the 1994 Northridge California earthquake recorded at the LABSN Station 00003 Northridge–17645 Saticoy Street station (rupture distance [R_{rup}] = 12 km, average shear-wave velocity within 30 m depth [V_{S30}] = 281 m/s) and at CGS–CSMIP Station 25091 Santa Barbara–UCSB Goleta (R_{rup} = 109 km, V_{S30} = 339 m/s) and their wavelet packet coefficients. The duration of the Saticoy Street recording is shorter than that of the UCSB Goleta recording, so amplitudes of wavelet packet coefficients of the Saticoy Street recording are large for a shorter window of time than in the UCSB Goleta recording. In the UCSB Goleta recording, the wavelet packets with high frequencies have very low amplitudes late in the recording. This is because the high-frequency components of seismic motions attenuate more rapidly with distance than the low-frequency components and the latter waves include indirect waves that travel longer distances than the direct waves, and thus have lower frequency. This reasonably explains the observation in Figure 2 that spectral nonstationarity in the UCSB Goleta recording is stronger than that in the Saticoy Street recording. To describe this time and frequency nonstationarity, we compute the correlation coefficient between the time and frequency of the wavelet packet coefficients $\rho(t, f)$, as discussed in the following section. For these examples, $\rho(t, f)$ in the Saticoy Street recording is −0.07 and in the UCSB Goleta recording is −0.34.

Stochastic Model of Ground Motion Using WPT

The WPT is a compressive transform that results in typical time series having only a few wavelet packet coefficients with large amplitude and many small or near-zero amplitude coefficients. To take advantage of this compression, and to distinguish between large- and small-amplitude packets, our model defines two groups of wavelet packet coefficients (termed the major and minor groups of packets). The total wavelet packet coefficients are a combination of these two groups as follows:

$$|c^i_{j,k}|^2 = |c^i_{j,k,\mathrm{maj}}|^2 + |c^i_{j,k,\mathrm{min}}|^2, \tag{5}$$

in which $c^i_{j,k,\mathrm{maj}}$ and $c^i_{j,k,\mathrm{min}}$ are the wavelet packet coefficients in the major and minor groups, respectively.

The major group of wavelet packet coefficients consists of the largest amplitude coefficients, which together contains 70% of the total energy in the ground motion (typically this is less than 1% of the total number of wavelet packet coefficients). The remaining smaller packets are in the minor group. The energy fraction used in separating the major group was determined by varying this fraction until the difference of the characteristics (duration, bandwidth, and mean frequency) of wavelet packet coefficients of the major and minor groups was maximized.

To quantify the time and frequency characteristics of the acceleration time series, we define the following 13 parameters: for the major group, (1) temporal centroid $E(t)_{\mathrm{maj}}$, (2) temporal variance $S^2(t)_{\mathrm{maj}}$, (3) spectral centroid $E(f)_{\mathrm{maj}}$, (4) spectral variance $S^2(f)_{\mathrm{maj}}$, (5) correlation between time and frequency of wavelet packet coefficients $\rho(t,f)_{\mathrm{maj}}$, (6) mean of squared amplitudes of the wavelet packet coefficients $E(a)_{\mathrm{maj}}$; and for the minor group, (7) temporal centroid $E(t)_{\mathrm{min}}$, (8) temporal variance $S^2(t)_{\mathrm{min}}$, (9) spectral centroid $E(f)_{\mathrm{min}}$, (10) spectral variance $S^2(f)_{\mathrm{min}}$, (11) correlation between time and frequency of wavelet packet coefficients $\rho(t,f)_{\mathrm{min}}$, (12) randomness of amplitude of wavelet packets $S(\xi)$, and for the total wavelet packet coefficients, and (13) cumulative squared acceleration E_{acc}. The following equations define these parameters and Figure 3 shows the relationship between wavelet packet coefficients and some of these parameters:

$$E_{\mathrm{acc}} = \sum_i \sum_k |c^i_{j,k}|^2 = \int_{-\infty}^{\infty} |x(t)|^2 dt, \tag{6}$$

$$E(a)_{\mathrm{maj}} = \sum_i \sum_k |c^i_{j,k,\mathrm{maj}}|^2 / n_{\mathrm{maj}}, \tag{7}$$

$$E(t)_{\mathrm{maj}} = \sum_i \sum_k t_{i,k,\mathrm{maj}} / n_{\mathrm{maj}}, \tag{8}$$

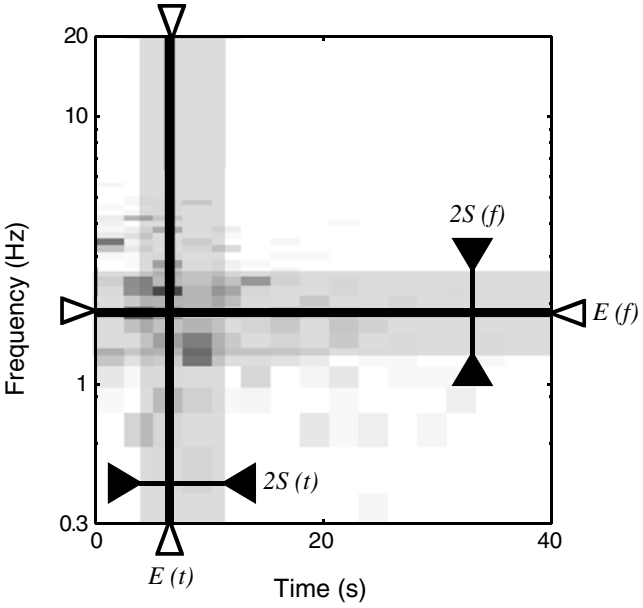

Figure 3. Plot of the wavelet packet coefficients from the UCSB Goleta recording, indicating the relationship between the parameters, $E(t)$, $S(t)$, $E(f)$, and $S(f)$, and the wavelet packet coefficients.

$$S^2(t)_{\mathrm{maj}} = \sum_i \sum_k \{t_{i,k,\mathrm{maj}} - E(t)_{\mathrm{maj}}\}^2 / (n_{\mathrm{maj}} - 1), \tag{9}$$

$$E(f)_{\mathrm{maj}} = \sum_i \sum_k f_{i,k,\mathrm{maj}} / n_{\mathrm{maj}}, \tag{10}$$

$$S^2(f)_{\mathrm{maj}} = \sum_i \sum_k \{f_{i,k,\mathrm{maj}} - E(f)_{\mathrm{maj}}\}^2 / (n_{\mathrm{maj}} - 1), \tag{11}$$

$$\rho(t,f)_{\mathrm{maj}} = \frac{\sum_i \sum_k [t_{i,k,\mathrm{maj}} - E(t)_{\mathrm{maj}}][f_{i,k,\mathrm{maj}} - E(f)_{\mathrm{maj}}]}{S(t)_{\mathrm{maj}} S(f)_{\mathrm{maj}} (n_{\mathrm{maj}} - 1)}, \tag{12}$$

in which n_{maj} is number of wavelet packet coefficients, and $t_{i,k,\mathrm{maj}}$ and $f_{i,k,\mathrm{maj}}$ are the center of the time and frequency location of a wavelet packet coefficient in the major group, respectively;

$$E(t)_{\mathrm{min}} = \sum_i \sum_k t_{i,k,\mathrm{min}} |c^i_{j,k,\mathrm{min}}|^2 / (0.3 E_{\mathrm{acc}}), \tag{13}$$

$$S^2(t)_{\mathrm{min}} = \sum_i \sum_k \{t_{i,k,\mathrm{min}} - E(t)_{\mathrm{min}}\}^2 |c^i_{j,k,\mathrm{min}}|^2 / (0.3 E_{\mathrm{acc}}), \tag{14}$$

$$E(f)_{\min} = \sum_i \sum_k f_{i,k,\min} |c^i_{j,k,\min}|^2 / (0.3E_{\text{acc}}), \quad (15)$$

$$S^2(f)_{\min} = \sum_i \sum_k \{f_{i,k,\min} - E(f)_{\min}\}^2 |c^i_{j,k,\min}|^2 / (0.3E_{\text{acc}}), \quad (16)$$

$$\rho(t,f) = \frac{\sum_i \sum_k [t_{i,k,\min} - E(t)_{\min}][f_{i,k,\min} - E(f)_{\min}] |c^i_{j,k,\min}|^2}{0.3E_{\text{acc}} S(t)_{\min} S(f)_{\min}}, \quad (17)$$

in which $t_{i,k,\min}$ and $f_{i,k,\min}$ are the center of the time and frequency location of a wavelet packet coefficient in the minor group, respectively.

Major Group of Wavelet Packets

Statistical studies of major wavelet packet coefficients indicated that their locations in time and frequency are dependent, but that their locations are independent from their amplitudes. Further, the squared amplitudes appear to be well represented by exponential distributions and the locations appear to be consistent with bivariate lognormal distributions. So the amplitudes and locations of these coefficients are modeled using the following probability distributions

$$a_{\text{maj}} \sim \text{Exponential}[E(a)_{\text{maj}}], \quad (18)$$

$$(\, t_{\text{maj}} \quad f_{\text{maj}} \,) \sim \text{Lognormal}(M_{\text{maj}}, \Sigma_{\text{maj}}), \quad (19)$$

in which $\sim$ denotes that the variable has the specified distribution, a_{maj} is the squared amplitude of a wavelet packet coefficient in the major group c_{maj}, and t_{maj} and f_{maj} are the center of the time and frequency location of a wavelet packet coefficient in the major group, respectively. If we define X and Y as the natural log of time and frequency:

$$X = \ln(t_{\text{maj}}), \qquad Y = \ln(f_{\text{maj}}), \quad (20)$$

then M_{maj} and Σ_{maj} are defined by

$$M_{\text{maj}} = \begin{bmatrix} E(X) & E(Y) \end{bmatrix}, \quad (21)$$

$$\Sigma_{\text{maj}} = \begin{bmatrix} S^2(X) & \text{Cov}(X,Y) \\ \text{Cov}(X,Y) & S^2(Y) \end{bmatrix}, \quad (22)$$

in which $E(X)$ and $E(Y)$ are means of $\ln(t_{\text{maj}})$ and $\ln(f_{\text{maj}})$, $S(X)$ and $S(Y)$ are standard deviations of $\ln(t_{\text{maj}})$ and $\ln(f_{\text{maj}})$, and $\text{Cov}(X,Y)$ is covariance of $\ln(t_{\text{maj}})$ and $\ln(f_{\text{maj}})$, which can be computed by the parameters in equations (8)–(12). The squared amplitudes of wavelet packets at the time t_{maj} and the frequency f_{maj} are independent and identically distributed (i.i.d.) exponential random variables with mean $E(a)$, and their time and frequency locations, t_{maj} and f_{maj}, are also i.i.d. bivariate lognormal random variables.

Minor Group of Wavelet Packets

Motivated by the past use of lognormal distributions to model ground-motion Fourier amplitudes (e.g., Thráinsson and Kiremidjian, 2002), here we use the lognormal distribution to model the frequency characteristics of the wavelet packet coefficients. The median amplitudes of the minor group of the wavelet packet coefficients are represented by a bivariate lognormal probability density function (PDF) as a function of the time and frequency, with a residual term adding variability about that median amplitude.

First, we define X and Y as the natural log of time and frequency locations of wavelet packets:

$$X = \ln(t_{\min}), \qquad Y = \ln(f_{\min}). \quad (23)$$

The model for $|c_{\min}|^2$ is then defined as follows:

$$|c_{\min}|^2 = \frac{1}{2\pi S(X) S(Y) \sqrt{[1-\rho(X,Y)^2]}} \times \frac{1}{t_{\min} f_{\min}} \exp\left\{ -\frac{A^2 - 2\rho(X,Y)AB + B^2}{2[1-\rho^2(X,Y)]} \right\} \times 0.3E_{\text{acc}} \times \xi, \quad (24)$$

in which A and B are defined as

$$A = \frac{X - E(X)}{S(X)}, \qquad B = \frac{Y - E(Y)}{S(Y)}, \quad (25)$$

and $c_{\min}$ is a minor wavelet packet coefficient at the time $t_{\min}$ and the frequency $f_{\min}$, $\rho(X,Y)$ is the correlation coefficient of $\ln(t_{\min})$ and $\ln(f_{\min})$, $E(X)$ and $E(Y)$ are means of $\ln(t_{\min})$ and $\ln(f_{\min})$, $S(X)$ and $S(Y)$ are standard deviations of $\ln(t_{\min})$ and $\ln(f_{\min})$, which can be computed by the parameters in equations (13)–(17), and E_{acc} is cumulative acceleration from equation (6). The parameter ξ is a lognormal random variable with median one and standard deviation that is calibrated below. With this model, a bivariate lognormal PDF has been used to specify the median amplitude of the squared wavelet coefficient at a given time and frequency. The random variable ξ is then used to specify variability of the amplitudes around that median. $|c_{\min}|^2$ is thus a random variable, from which samples can be drawn when simulating ground motions. A random sign (positive or negative) is applied to each wavelet packet coefficient and a variety of tests suggested that this produces realistic time series.

Simulated Ground Motions

We estimated the 13 model parameters defined above for the Saticoy Street and UCSB Goleta recordings of the 1994

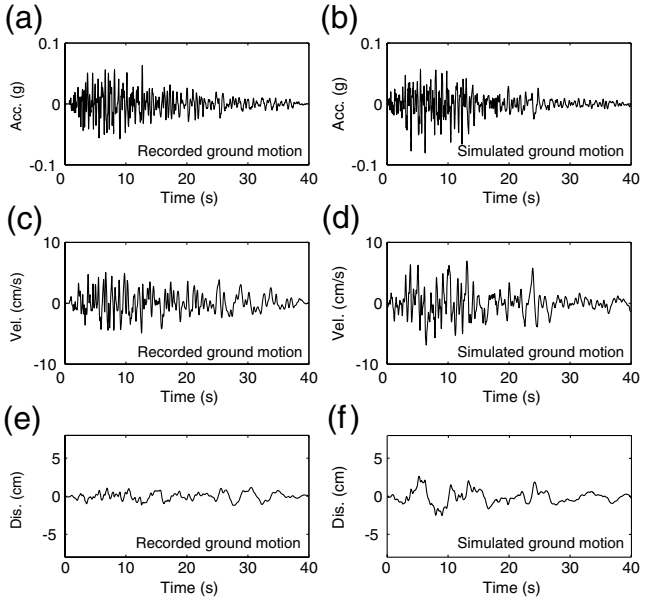

Figure 4. Recorded and simulated ground motion of the Northridge California earthquake at LABSN Station 00003 Northridge–17645 Saticoy Street (a) and (b) acceleration (g), and (c) and (d) velocity (cm/s) for recorded and simulated ground motion, respectively.

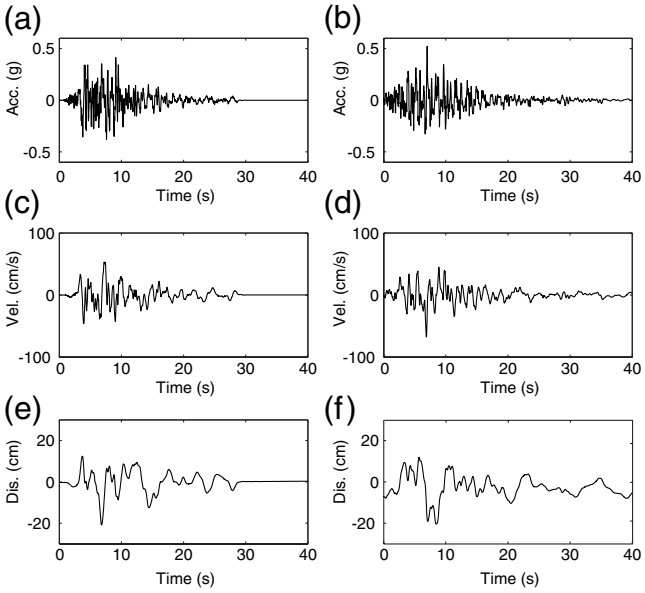

Figure 5. Recorded and simulated ground motion of the 1994 Northridge California earthquake at CGS–CSMIP Station 25091 Santa Barbara–UCSB Goleta (a) and (b) acceleration (g), and (c) and (d) velocity (cm/s) for recorded and simulated ground motion, respectively.

Northridge California earthquake, and then simulated wavelet packet coefficients (and resulting time series) using the above equations. Example acceleration, velocity, and displacement time series of simulated ground motions are shown in Figures 4 and 5, in comparison with the original recorded ground motions. The waveforms and peak accelerations, velocities, and displacements of the simulated ground motions reasonably match those of the recorded ground motions, and more extensive testing of this type showed similar results. This provides some indication that the above parameterization provides an accurate characterization of nonstationary earthquake ground motions.

Regression Analysis of Model Parameters

To generate a ground motion representing a particular earthquake scenario (i.e., magnitude, rupture location, and site condition), the 13 parameters for our model need to be predicted as a function of those scenario parameters. To build this predictive model, two-stage regression analysis (Joyner and Boore, 1993, 1994) is employed with moment magnitude (M_w), hypocentral distance (R_{hyp}), rupture distance (R_{rup}), and average shear-wave velocity within 30 m depth (V_{S30}) as predictor variables.

The recorded ground motions for the regression analysis come from the Next Generation of Attenuation (NGA) database (Chiou *et al.*, 2008). The model presented here is for fault-normal ground motions, and captures pulses sometimes observed in that component due to directivity, so fault-normal ground motions are selected from a subset of NGA database used by Boore and Atkinson (2008) with a lowest usable frequency less than or equal to 1 Hz. Additionally, ground motions from that data set are only used if the causal earthquake had at least ten recorded ground motions (in order to stabilize the two-stage regression analysis). These criteria result in 1408 ground motions from 25 earthquakes being used. For each ground motion, the 13 model parameters are estimated using the maximum likelihood estimation (accounting for frequency truncation due to filtering and a time-shift trigger-time correction, Yamamoto and Baker, 2011). The correlations of time and frequency in the major and minor groups are transformed by the following equation because they are bounded at -1 and 1:

$$\rho' = \Phi^{-1}\left(\frac{\rho + 1}{2}\right), \tag{26}$$

in which Φ is the cumulative density function of the standard normal distribution, ρ is the estimated correlation coefficient, and ρ' is the transformed (and unbounded) coefficient that is more suitable for prediction using regression equations.

The following functional form is used to predict the model parameters, and is motivated in part by functions used in modern GMPEs

$$Y = \alpha + \beta_1 M + \beta_2 \ln(M) + \beta_3 \exp(M) + \beta_4 (R_{hyp} - R_{rup}) + \beta_5 \ln\left(\sqrt{R_{rup}^2 + h^2}\right) + \beta_6 \ln(V_{S30}) + \eta + \delta, \tag{27}$$

in which Y is the natural logarithm of a model parameter (except for the case of correlation, for which $Y = \rho'$), and η and δ are intra- and interevent residuals, respectively. The parameters α and β_i are regression coefficients to be estimated.

Table 1
Coefficients of the Prediction Equation

Parameter to be Predicted	α	β_1 M	β_2 $\ln(M)$	β_3 $\exp(M)$	β_4 $R_{hyp}-R_{rup}$	β_5 $\ln(\sqrt{R_{rup}^2+h^2})$	β_6 $\ln(V_{S30})$	h	σ	τ	σ^*
$E(t)_{min}$	2.64	N/A	N/A	0.0004	−0.001	0.22	−0.16	1	0.18	0.21	0.28
$S(t)_{min}$	3.06	N/A	N/A	0.0004	−0.005	0.11	−0.17	1	0.21	0.23	0.31
$E(f)_{min}$	1.29	−0.14	N/A	N/A	−0.004	−0.23	0.36	10	0.35	0.26	0.44
$S(f)_{min}$	1.48	−0.005	N/A	N/A	−0.003	−0.29	0.24	10	0.40	0.29	0.49
$\rho'(t,f)_{min}$	−0.36	0.01	N/A	N/A	−0.00056	−0.03	0.04	10	0.06	0.03	0.06
$E(t)_{maj}$	1.95	N/A	N/A	0.0006	−0.002	0.34	−0.20	1	0.27	0.30	0.40
$S(t)_{maj}$	1.82	N/A	N/A	0.0006	−0.006	0.22	−0.20	1	0.34	0.33	0.48
$E(f)_{maj}$	0.81	−0.26	N/A	N/A	−0.004	−0.16	0.44	10	0.41	0.26	0.48
$S(f)_{maj}$	0.14	−0.12	N/A	N/A	−0.002	−0.24	0.39	10	0.56	0.37	0.68
$\rho'(t,f)_{maj}$	−0.54	0.01	N/A	N/A	−0.00008	−0.08	0.09	10	0.21	0.07	0.22
$E(a)_{maj}$	−38.02	−4.52	37.30	N/A	N/A	−1.74	−0.94	10	1.13	0.71	1.33
E_{acc}	−27.4	−2.58	27.00	N/A	N/A	−1.61	−0.88	10	0.85	0.46	0.96
$S(\xi)$	1.29	N/A	N/A	N/A	N/A	N/A	N/A	N/A	0.07	N/A	0.07

The parameter h is assigned to avoid predicting extremely large values of Y for small values of R_{rup}, and is determined by minimizing the mean square error of the regression predictions. With this functional form, R_{rup} predicts the attenuation of the motion with distance. The second distance parameter, R_{hyp}, only appears as a difference of distances, $R_{hyp}-R_{rup}$, which is a proxy for the rupture length between the hypocenter and the site. The $R_{hyp}-R_{rup}$ term does not predict attenuation of ground motion, and the use of the difference between these distance metrics avoids numerical problems caused by R_{hyp} and R_{rup} being correlated for a given ground motion. More detailed discussion of the motivation for this functional form, its physical interpretation, and its implications at the boundaries of the observed data, is provided in Yamamoto and Baker (2011).

Three functional forms for magnitude scaling are employed in the general regression equation, though only some of them are used depending upon the particular model parameter being considered. For the model parameters related to the characteristics in the time domain, $\exp(M)$ is used as it was observed to be consistent with the empirical data for those parameters. The linear M term is used for the model parameters related to the characteristics in the frequency domain, and is motivated by the relationship between magnitude and corner frequency f_c (Brune, 1970), which determines the frequency characteristics of the fault rupture. Also, M is used for prediction of $E(a)$ and E_{acc}, based on the relationship between magnitude and seismic moment (Kanamori, 1977), which is a measure of energy released by the rupture. The logarithmic $\ln(M)$ term is also employed for prediction of $E(a)$ and E_{acc}, because these parameters saturate at large magnitudes.

The uncertainty terms, η and δ, are normally distributed, with mean zero and standard deviations of τ and σ, and they are assumed to be independent for each ground motion (though they are correlated between parameters for a given ground motion). Therefore, standard deviation of total residual term σ^* is defined as follows:

$$\sigma^* = \sqrt{\tau^2+\sigma^2}. \tag{28}$$

With this general functional form, regression analysis was then performed to predict each of the 13 model parameters for each of the 1408 ground motions. After an initial regression analysis, statistically insignificant predictor variables were removed from the function and regression was rerun. A number of regression diagnostic tests were also performed to verify the reasonableness of the functional forms, the potential value of additional predictor variables, and the normality of the residual terms. After refinement of the model, the resulting regression coefficients are shown in Table 1, and the correlations of total residuals for each pair of parameters are shown in Table 2. Regression coefficients that are not used for each model parameter are set to N/A in Table 1. The model parameters are correlated through the intra- and interevent residuals because the model parameters computed from recorded ground motions are jointly affected by factors not fully accounted for by the proposed regression model.

The signs and amplitudes of the regression coefficients are generally consistent with seismology theory and empirical observations of ground-motion properties. A few examples are provided here to illustrate these consistencies. For the parameters related to time-axis properties, values of β_3 are positive, because earthquakes with large magnitudes have longer durations and thus also later temporal centroids. Values of β_5 are also positive for the time-axis parameters, because waves propagating over long distances have scattered arrivals and include indirect waves as well as direct waves, leading to increased durations. Similarly, soft soils tend to increase durations, leading to negative coefficients for β_6 for the time-axis parameters. The regression coefficients for β_4 are negative for these parameters because large

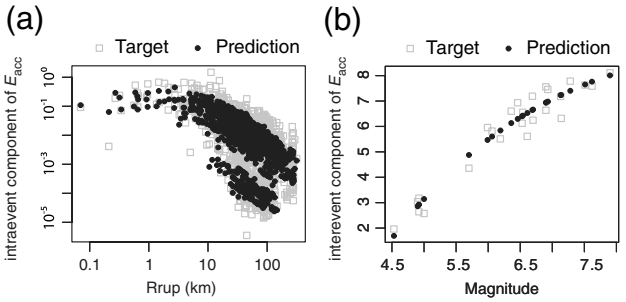

Figure 6. Median prediction of regression analysis (a) intraevent component of E_{acc}, (b) interevent component of E_{acc}.

values of $R_{hyp} - R_{rup}$ are associated with forward directivity, leading to shorter durations.

For the parameters related to the frequency axis, values of β_1 are negative, because earthquakes with large magnitudes have low corner frequencies (Brune, 1970). The effect of magnitude is stronger for $E(f)$ than $S(f)$, as expected. Values of β_5 are negative because longer wave propagation distance reduces $E(f)$ and $S(f)$ as high-frequency ground-motion components attenuate more quickly with distance than low-frequency components. β_4 is negative for $E(f)$ because a greater difference between hypocentral distance and rupture distance is associated with forward directivity (Boatwright and Boore, 1982). β_6 is positive for $E(f)$ and $S(f)$ because the natural frequency of stiff soil is higher than that of soft soil, and stiff soils tend to produce more broadband motions.

For the time-frequency nonstationarity term $\rho'(t,f)$, β_5 is negative because with increasing distance the higher-frequency components of ground motions arrive earlier than the lower-frequency components, and because the later-arriving indirect waves have less high-frequency energy due to attenuation. These factors result in greater nonstationarity, as reflected by a larger amplitude (i.e., more negative) $\rho'(t,f)$.

The mean energy E_{acc} decreases with distance due to attenuation, as illustrated in Figure 6a, and increases for small V_{S30} due to site amplification. Also, E_{acc} increases with magnitude and saturates at large magnitudes, as seen in Figure 6b. The trend of $E(a)_{maj}$ is the same as that of E_{acc}. Additional related results and documentation of the regression analysis is provided in Yamamoto and Baker (2011).

Comparison of Simulation Results with GMPEs

Simulated ground motions generated by the proposed model are next compared with the properties of recorded ground motions as predicted by existing GMPEs. The 5%-damped spectral accelerations (S_a) of the simulated ground motions are compared with those from NGA GMPEs calibrated using similar data to that used here (Abrahamson and Silva, 2008 [AS08]; Boore and Atkinson, 2008 [BA08]; Campbell and Bozorgnia, 2008 [CB08]; Chiou and Youngs, 2008 [CY08]; Idriss, 2008 [I08]). The residuals (ε) of recorded ground motions are studied to determine whether they are normally distributed by Jayaram and Baker (2008) and the inter-period correlations of the ε's are compared with predictions by Baker and Jayaram (2008). Selected additional comparisons of this type for Arias intensity, mean period, and significant duration are also shown.

The 5%-damped spectral accelerations are predicted directly by GMPEs, whereas the model proposed here predicts time series and the S_a values are only an indirect result of the simulated motions. Therefore, the proposed model cannot be directly calibrated to produce S_a values consistent with recordings. Despite this difficulty with calibrating the proposed model, realistic S_a values must be produced in order for the model to be considered validated.

To evaluate the proposed regression equations and resulting simulations, 300 simulated ground motions are computed for each magnitude, distance, and site condition of interest, and their S_a values are computed and compared with the values predicted by GMPEs for the same condition.

In this paper, response-spectra comparisons are performed for vertical strike-slip faults under a variety of earthquake magnitudes, distances, and site conditions. The NGA models include additional predictor variables other than those used by the model proposed here, so to facilitate

Table 2
Correlation of Total Residuals

Parameter	$E(t)_{min}$	$S(t)_{min}$	$E(f)_{min}$	$S(f)_{min}$	$\rho'(t,f)_{min}$	$E(t)_{maj}$	$S(t)_{maj}$	$E(f)_{maj}$	$S(f)_{maj}$	$\rho'(t,f)_{maj}$	$E(a)_{maj}$	E_{acc}
$E(t)_{min}$	1.00	0.86	−0.24	−0.05	−0.43	0.88	0.69	−0.33	−0.13	−0.24	−0.32	−0.14
$S(t)_{min}$	0.86	1.00	−0.17	0.02	−0.43	0.66	0.74	−0.26	−0.04	−0.25	−0.41	−0.22
$E(f)_{min}$	−0.24	−0.17	1.00	0.86	0.17	−0.19	−0.09	0.88	0.83	0.09	−0.36	−0.15
$S(f)_{min}$	−0.05	0.02	0.86	1.00	−0.01	−0.03	0.08	0.67	0.81	−0.05	−0.47	−0.26
$\rho'(t,f)_{min}$	−0.43	−0.43	0.17	−0.01	1.00	−0.33	−0.35	0.19	−0.01	0.56	0.14	0.06
$E(t)_{maj}$	0.88	0.66	−0.19	−0.03	−0.33	1.00	0.69	−0.30	−0.13	−0.26	−0.29	−0.16
$S(t)_{maj}$	0.69	0.74	−0.09	0.08	−0.35	0.69	1.00	−0.21	0.02	−0.28	−0.46	−0.29
$E(f)_{maj}$	−0.33	−0.26	0.88	0.67	0.19	−0.30	−0.21	1.00	0.83	0.11	−0.28	−0.09
$S(f)_{maj}$	−0.13	−0.04	0.83	0.81	−0.01	−0.13	0.02	0.83	1.00	−0.05	−0.49	−0.23
$\rho'(t,f)_{maj}$	−0.24	−0.25	0.09	−0.05	0.56	−0.26	−0.28	0.11	−0.05	1.00	0.14	0.08
$E(a)_{maj}$	−0.32	−0.41	−0.36	−0.47	0.14	−0.29	−0.46	−0.28	−0.49	0.14	1.00	0.87
E_{acc}	0.14	0.22	0.15	0.26	0.06	0.16	0.29	0.09	0.23	0.08	0.87	1.00

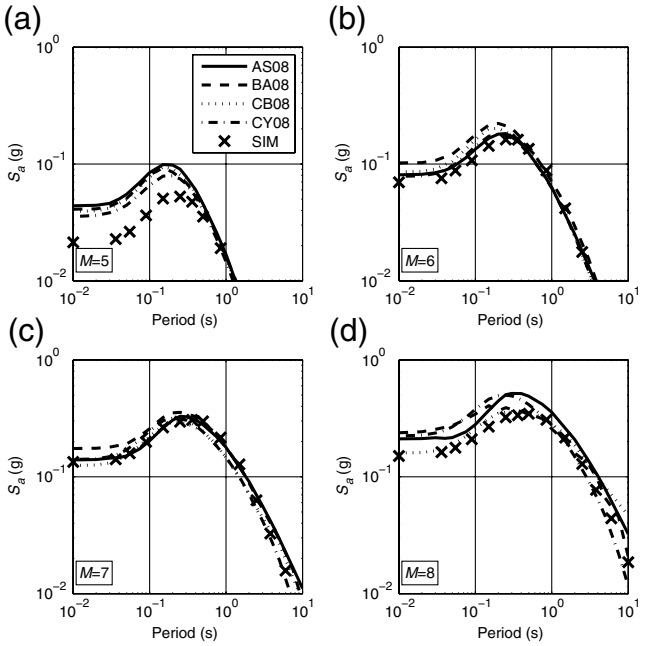

Figure 7. Median of elastic S_a computed from the NGA GMPEs and simulations ($R_{JB} = 30$ km, $V_{S30} = 270$ m/s) for (a) M 5, (b) M 6, (c) M 7, and (d) M 8.

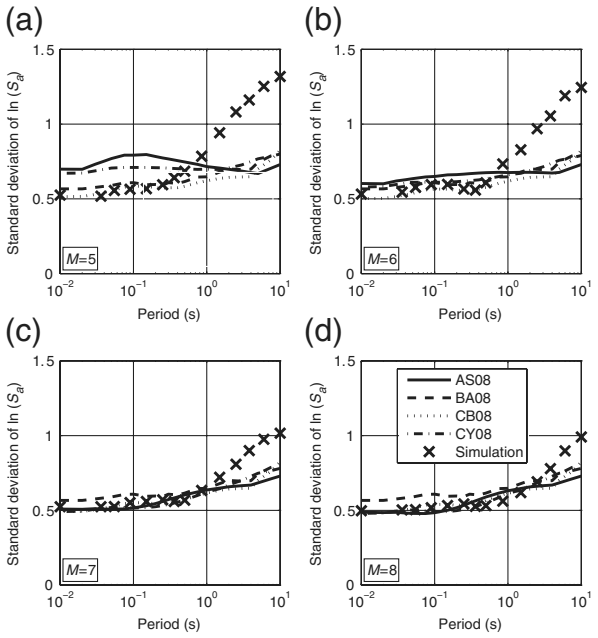

Figure 8. Logarithmic standard deviation of elastic S_a computed from the NGA GMPEs and simulations ($R_{JB} = 30$ km, $V_{S30} = 270$ m/s). (a) M 5, (b) M 6, (c) M 7, and (d) M 8.

comparisons with the NGA predictions we use a depth-to-top-of-rupture (Z_{tor}) of 6 km for M 5, 3 km for M 6, 1 km for M 7, and 0 km for M 8 based on the recommendation of Abrahamson *et al.* (2008), and R_{rup} is defined by the depth-to-top-of-rupture and R_{JB} as follows:

$$R_{rup} = \sqrt{R_{JB}^2 + Z_{tor}^2}. \tag{29}$$

$Z_{1.0}$ values are inferred from V_{S30} using the suggested approaches by individual models. $Z_{1.0}$ for AS08 are from Abrahamson and Silva (2008), and $Z_{1.0}$ for CY08 is defined using the following equation from Chiou and Youngs (2008)

$$\ln(Z_{1.0}) = 28.5 - \frac{3.82}{8}\ln(V_{S30}^8 + 378.7^8). \tag{30}$$

Spectral Acceleration

The median response spectra for M 5, 6, 7, and 8 at sites with $R_{JB} = 30$ km and $V_{S30} = 270$ m/s are shown in Figure 7. The S_a from the simulated ground motions reasonably match those from GMPEs, especially for M 6, 7, and 8, which are likely to be of greatest engineering interest. The logarithmic standard deviations of response spectra for the same conditions as Figure 7 are shown in Figure 8. For all cases, standard deviations from simulations are consistent with GMPEs at short-to-moderate periods, but larger than those from GMPEs at long periods.

The logarithmic standard deviations of S_a increase with period in the simulations for all magnitudes. Careful study of the simulations shows that the logarithmic standard deviations start increasing at the peak period of the response spectrum, which is associated with the spectral centroid of the wavelet packet coefficients in both the major and minor groups. S_a at short periods has smaller logarithmic standard deviations than at long periods because short period S_a is controlled by peak amplitude based on the shape of the transfer function. Additionally, we have uncertainty in the spectral centroid, so the fluctuation of the peak period affects the logarithmic standard deviation of S_a around the peak of S_a. Hence, at periods greater than the peak S_a, the logarithmic standard deviations significantly increase with period.

A second explanation for this increase in standard deviation is that the wavelet transform has limited period resolution at these long periods, due to its finite time-domain resolution. These large standard deviations of $\ln S_a$ at long periods are a weakness of the proposed stochastic model. Although the problem is most severe at long periods for small-magnitude earthquakes, which are of less engineering interest, the problem is still somewhat present for large-magnitude earthquakes. The limitations of the model observed in Figures 7 and 8 will be used to constrain the recommended range of applicability of the model, as discussed later.

Correlation of Epsilon

The residual of $\ln S_a$ from the mean prediction (ε) is defined by the following equation:

$$\varepsilon(T) = \frac{\ln S_a(T) - \mu_{\ln S_a(T)}(M, R, T)}{\sigma_{\ln S_a(T)}}, \tag{31}$$

in which S_a is the spectral acceleration observed from a ground motion, $\mu_{\ln S_a}$ is the mean predicted logarithmic spectral acceleration, and $\sigma_{\ln S_a}$ is the logarithmic standard

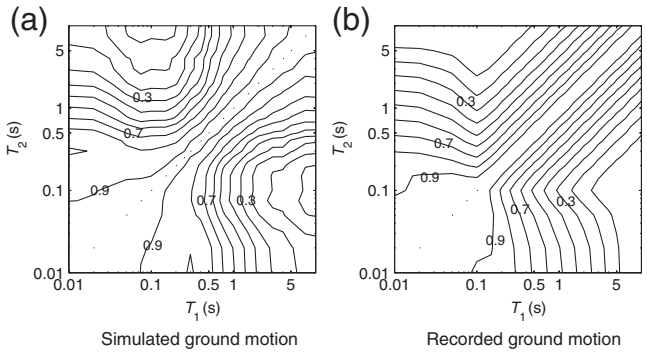

Figure 9. Contour of correlation coefficients versus ε for T_1 and T_2. (a) Empirical correlation coefficients computed from the simulated ground motions, (b) correlation coefficients computed by Baker and Jayaram (2008).

deviation of the spectral acceleration. This ε is an implicit indicator of the shape of the response spectrum, and correlations between ε at differing periods can be used to quantify the "bumpiness" of the spectrum (Baker and Cornell, 2005).

Correlation of ε at different periods, as observed from recorded ground motions, are modeled by, for example, Baker and Jayaram (2008). Figure 9 shows contours of correlations of ε from our simulations and those from Baker and Jayaram (2008), and the two are seen to match closely. One of the reasons for this good agreement is the WPT approach that we are using for our model. The kernel function of the wavelet packet is localized in a range of time and frequency, and therefore, the response spectrum of the kernel function is also localized in a narrow range of periods. Hence, correlations of ε in different periods with small period differences are high and they decrease as the period difference increases. Some other methods for stochastic simulation of ground motions are known to not reproduce the correlations of ε's observed in real ground motions (Tothong and Cornell, 2007; Sadeghi *et al.*, 2011), so the ability of this approach to do so is a very positive feature.

Other Parameters

Inelastic response spectra are computed for M 7, vertical strike-slip fault, and $V_{S30} = 270$ m/s for Joyner–Boore distances ranging from 1 to 100 km. The inelastic response spectrum here is defined as F_y/W (where F_y is the yield strength and W is the weight of the single degree-of-freedom system), and is computed for elastic-perfectly-plastic systems with 5% viscous damping ratio and ductility ratio $\mu = 8$ (Chopra, 2007). Figure 10 shows the median and logarithmic standard deviation of F_y/W, for both the ground motions produced by our model and the predictions from Bozorgnia *et al.* (2010). The results from our simulations match well with those from Bozorgnia *et al.* (2010), except for the $T = 3$ s results at small distances from the rupture. This discrepancy occurs in part because the wavelet packets at low frequencies have low resolution in the frequency domain, and so the fluctuation of the amplitude and frequency

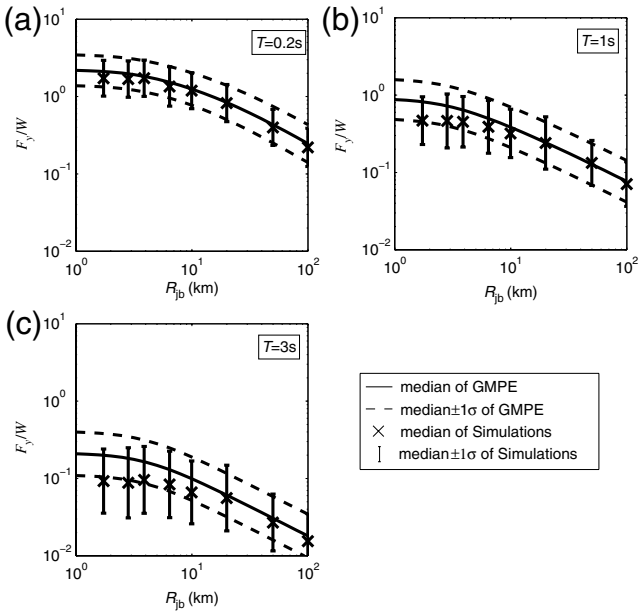

Figure 10. Median $\pm\sigma$ bounds of F_y/W with ductility $\mu = 8$ computed from the GMPE and simulations. (a) S_a at $T = 0.2$ s, (b) S_a at $T = 1$ s, and (c) S_a at $T = 3$ s.

of wavelet packets at long periods causes large variations in inelastic responses.

The parameters such as Arias intensity (I_a, Arias, 1970), mean period (T_m, Rathje *et al.* 2004), and significant duration (t_{5-95}, Trifunac and Brady, 1976) are computed for an M 7, vertical strike-slip fault with $V_{S30} = 270$ m/s, and $1 \le R_{\text{rup}} \le 100$ km. Figure 11 shows the medians and logarithmic standard deviations of t_{95}, T_m, I_a observed from the simulations and predicted by corresponding GMPEs. All of these parameters from the simulations reasonably match those from GMPE predictions.

Conclusions

This paper documented the construction of a stochastic ground-motion model with time-frequency nonstationarity based on the WPT. The time- and frequency-varying properties of real ground motions are modeled using wavelet packet coefficients, and the proposed model requires 13 parameters to describe a given ground motion. These 13 model parameters are then related to seismological variables such as earthquake magnitude and distance, through a two-stage regression analysis that captures trends in mean values, variabilities, and correlations of these parameters observed in a large database of recorded strong ground motions.

The proposed model has the following advantages: (a) the temporal and the spectral nonstationarity of the simulated motions can be fully controlled by adjusting the model parameters, (b) the model is empirically calibrated and produces motions that are consistent with observed ground-motion recordings in terms of properties of engineering interest, and (c) the procedure is computationally inexpensive

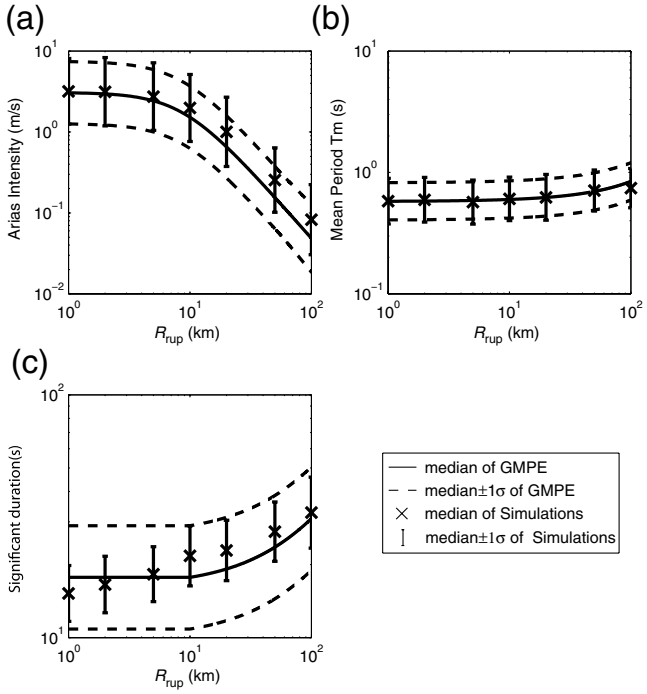

Figure 11. Median $\pm\sigma$ bounds of other ground-motion parameters computed from GMPEs and simulations. (a) Simulated I_a and predictions from Travasarou *et al.* (2003), (b) simulated T_m and predictions from Rathje *et al.* (2004), and (c) simulated t_{5-95} and predictions from Abrahamson and Silva (1996).

(1000 simulations per hour can be produced on a standard desktop PC), so obtaining large numbers of ground motions is relatively fast.

The characteristics of the resulting simulated ground motions were examined by comparing elastic and inelastic spectral acceleration values, Arias intensity, mean period, and significant duration observed in simulated ground motions with comparable predictions from GMPEs. The properties of the simulations were observed to reasonably match those from GMPEs for $6 \le M \le 8$, $220 \le V_{S30} \le 760$ m/s, $1 \le R_{rup} \le 100$ km, $0.01 \le T \le 3$ s, and vertical strike-slip faulting.

Furthermore, the characteristics of the prediction errors of S_a (i.e., ε) were examined. The characteristics of ε are related to the probabilistic characteristics of the spectral shape of ground motions. The prediction errors ε from simulations were seen to be normally distributed (as is also the case with recorded ground motions) and have correlations that are consistent with an existing empirical model calibrated from recordings.

While the simulated ground motions were observed to be reasonable over the range of conditions described above, there are some unresolved modeling issues that if improved could potentially increase the circumstances under which the simulations can be viewed as realistic. The proposed regression model has only four predictors: moment magnitude, hypocentral distance, rupture distance, and V_{S30}. For future improvement, we could consider including additional predictors such as rupture mechanism and depth to bedrock. Initial regression models considered did not indicate a statistically significant trend with any of these parameters, but their effectiveness in other GMPEs suggests that they may be useful predictors. The functional form used for regression was also kept relatively simple for practical purposes. For example, the parameter h employed in the proposed regression model controls saturation of each parameter in the near fault region. In the current model, h is constant for a given model parameter, but the model could be modified so h is a function of magnitude (because h is related to the area of the fault). Additionally, there are some weaknesses of the model with regard to long period energy, as was seen in plots of standard deviations of long period response spectra. This is in part an inherent limitation of any procedure that attempts to model long period energy in a finite-length signal, due to inherent limitations on time and frequency resolution in signal processing. Nonetheless, opportunities for incremental further improvements likely remain. Alternatively, the proposed procedure could be used to generate only the high-frequency components of ground motion, in a hybrid simulation that relied on physics-based simulations for low-frequency ground motion (e.g., Graves and Pitarka, 2010).

Despite some limitations, the ease of use of this procedure and general consistency of a number of properties of these simulations with comparable predictions of those properties by empirical prediction equations suggests that the simulations are suitable for probabilistic seismic-hazard analysis and perhaps nonlinear dynamic structural analysis.

Data and Resources

The recorded ground motions for the regression analysis come from the NGA database (Chiou *et al.*, 2008). The stochastic model described in this paper has been implemented in the MATLAB programming environment using the MATLAB Wavelet Toolbox. To supplement the documentation provided by this paper, the source code is available at www.stanford.edu/~bakerjw/gm_simulation.html (last accessed March 2013). The website also contains further detailed documentation such as regression coefficients, a table of earthquake ground motions used in regression analysis, and other relevant information for the validation of the model.

Acknowledgments

The authors thank Anne Kiremidjian and Eduardo Miranda for helpful comments on this work. The authors also thank two anonymous reviewers for their detailed and helpful comments on the manuscript. This material is based upon work supported by the National Science Foundation under NSF Grant Number CMMI 0726684. Any opinions, findings, and conclusions or recommendations expressed in this material are those of the authors and do not necessarily reflect the views of the National Science Foundation.

References

Abrahamson, N. A., and W. J. Silva (1996). *Empirical Ground Motion Models*, Brookhaven National Laboratory, Upton, New York, 144 pp.

Abrahamson, N. A., and W. J. Silva (2008). Summary of the Abrahamson & Silva NGA ground-motion relations, *Earthq. Spectra* **24,** no. 1, 67–97.

Abrahamson, N. A., G. Atkinson, D. Boore, Y. Bozorgnia, K. Campbell, B. Chiou, I. M. Idriss, W. J. Silva, and R. Youngs (2008). Comparisons of the NGA ground-motion relations, *Earthq. Spectra* **24,** no. 1, 45–66.

Alamilla, J., L. Esteva, J. Garcia-Perez, and O. Diaz-Lopes (2001). Evolutionary properties of stochastic models of earthquake accelerograms: Their dependence on magnitude and distance, *J. Seismol.* **5,** 1–21.

Amiri, G. G., A. Shahjouei, S. Saadat, and M. Ajallooeian (2011). Hybrid evolutionary-neural network approach in generation of artificial accelerograms using principal component analysis and wavelet-packet transform, *J. Earthq. Eng.* **15,** no. 1, 50–76.

Arias, A. (1970). A measure of earthquake intensity, in *Seismic Design for Nuclear Power Plants*, R. J. Hansen (Editor), MIT Press, Cambridge, Massachusetts, 438–483.

Baker, J. W., and C. A. Cornell (2005). A vector-valued ground motion intensity measure consisting of spectral acceleration and epsilon, *Earthq. Eng. Struct. Dyn.* **34,** no. 10, 1193–1217.

Baker, J. W., and N. Jayaram (2008). Correlation of spectral acceleration values from NGA ground motion models, *Earthq. Spectra* **24,** no. 1, 299–317.

Boatwright, J., and D. M. Boore (1982). Analysis of the ground accelerations radiated by the 1980 Livermore valley earthquakes for directivity and dynamic source characteristics, *Bull. Seismol. Soc. Am.* **72,** no. 6, 1843–1865.

Boore, D. M., and G. M. Atkinson (2008). Ground-Motion prediction equations for the average horizontal component of PGA, PGV, and 5%-Damped PSA at spectral periods between 0.01 s and 10.0 s, *Earthq. Spectra* **24,** no. 1, 99–138.

Bozorgnia, Y., M. M. Hachem, and K. W. Campbell (2010). Ground motion prediction equation ("Attenuation Relationship") for inelastic response spectra, *Earthq. Spectra* **26,** no. 1, 1–23.

Brune, J. N. (1970). Tectonic stress and the spectra of seismic shear waves from earthquakes, *J. Geophys. Res. Lett.* **75,** no. 26, 4997–5009.

Campbell, K. W., and Y. Bozorgnia (2008). NGA ground motion model for the geometric mean horizontal component of PGA, PGV, PGD and 5% damped linear elastic response spectra for periods ranging from 0.01 to 10 s, *Earthq. Spectra* **24,** no. 1, 139–171.

Chiou, B., and R. R. Youngs (2008). An NGA model for the average horizontal component of peak ground motion and response spectra, *Earthq. Spectra* **24,** no. 1, 173–215.

Chiou, B., R. Darragh, N. Gregor, and W. J. Silva (2008). NGA project strong-motion database, *Earthq. Spectra* **24,** no. 1, 23–44.

Chopra, A. K. (2007). *Dynamics of Structures*, Prentice Hall, Upper Saddle River, New Jersey, 876 pp.

Conte, J. P. (1992). Effects of earthquake frequency nonstationarity on inelastic structural response, in *Proc. of the 10th World Conference on Earthquake Engineering*, Madrid, Spain, July 1992, 3645–3651.

Cornell, C. A. (1964). *Stochastic Process Models in Structural Engineering*, Technical Report no. 34, Department of Civil Engineering, Stanford University, Stanford, California, 384 pp.

Douglas, J., and H. Aochi (2008). A survey of techniques for predicting earthquake ground motions for engineering purposes, *Surv. Geophys.* **29,** no. 3, 187–220.

Graves, R. W., and A. Pitarka (2010). Broadband ground-motion simulation using a hybrid approach, *Bull. Seismol. Soc. Am.* **100,** no. 5A, 2095–2123.

Hoshiya, M., and Z. Hasgur (1978). AR and MA models of nonstationary ground motion, *Bull. Int. Inst. Seismol. Earthq. Eng.* **16,** 55–68.

Idriss, I. M. (2008). An NGA empirical model for estimating the horizontal spectral values generated by shallow crustal earthquakes, *Earthq. Spectra* **24,** no. 1, 217–242.

Jayaram, N., and J. W. Baker (2008). Statistical tests of the joint distribution of spectral acceleration values, *Bull. Seismol. Soc. Am.* **98,** no. 5, 2231–2243.

Joyner, W. B., and D. M. Boore (1993). Methods for regression analysis of strong-motion data, *Bull. Seismol. Soc. Am.* **83,** no. 2, 469–487.

Joyner, W. B., and D. M. Boore (1994). Errata, methods for regression analysis of strong-motion data, *Bull. Seismol. Soc. Am.* **84,** no. 3, 955–956.

Kanamori, H. (1977). The energy release in great earthquake, *J. Geophys. Res.* **82,** no. 20, 2981–2987.

Lin, Y. K. (1986). On random pulse train and its evolutionary spectral representation, *Prob. Eng. Mech.* **1,** no. 4, 219–223.

Luco, N., and P. Bazzurro (2007). Does amplitude scaling of ground motion records result in biased nonlinear structural drift responses? *Earthq. Eng. Struct. Dynam.* **36,** no. 13, 1813–1835.

Masuda, A., and A. Sone (2002). Generation of spectrum-compatible earthquake motion using wavelet transform, in *ASME 2002 Pressure Vessels and Piping Conference 1*, Vancouver, BC, Canada, 5–9 August 2002.

Meyer, Y. (1986). Principe d'incertitude, bases hilbertiennes et algebres d'operateurs, *Séminaire N. Bourbaki* **662,** 209–223.

Nakamura, M., F. Sasaki, K. Yokoyama, and T. Tamaoki (2008). Generation of artificial earthquake motion using observed earthquake motions, in *Proc. of the 14th World Conference on Earthquake*, Beijing, China, 12–17 October 2008.

Page, C. H. (1952). Instantaneous power spectra, *J. Appl. Phys.* **23,** no. 1, 103–106.

Papadimitrios, K. (1990). Stochastic characterization of strong ground motion and applications to structural response, *Report NO. EERL 90-03*, Earthquake Engineering Research Laboratory, California Institute of Technology, Pasadena, California.

Pitarka, A., K. Irikura, T. Iwata, and H. Sekiguchi (1998). Three-dimensional simulation of the near-fault ground motion for the 1995 Hyogo-ken Nanbu (Kobe), Japan, Earthquake, *Bull. Seismol. Soc. Am.* **88,** no. 2, 428–440.

Pousse, G., L. F. Bonilla, F. Cotton, and L. Margerin (2006). Nonstationary stochastic simulation of strong ground motion time histories including natural variability: Application to the K-net Japanese database, *Bull. Seismol. Soc. Am.* **96,** no. 6, 2103–2117.

Priestley, M. B. (1965). Evolutionary spectra and non-stationary processes, *J. Roy. Stat. Soc. B Methodological* **27,** no. 2, 204–237.

Rathje, E. M., F. Faraj, S. Russell, and J. D. Bray (2004). Empirical relationships for frequency content parameters of earthquake ground motions, *Earthq. Spectra* **20,** no. 1, 119–144.

Rezaeian, S. (2010). *Stochastic Modeling and Simulation of Ground Motions for Performance-Based Earthquake Engineering*, Department of Civil and Environmental Engineering, University of California, Berkeley, California.

Rezaeian, S., and A. Der Kiureghian (2010). Simulation of synthetic ground motions for specified earthquake and site characteristics, *Earthq. Eng. Struct. Dynam.* **39,** no. 10, 1155–1180.

Rezaeian, S., and A. Der Kiureghian (2012). Simulation of orthogonal horizontal ground motion components for specified earthquake and site characteristics, *Earthq. Eng. Struct. Dynam.* **41,** no. 2, 335–353.

Sadeghi, M., A. Azarbakht, and M. Mousavi (2011). Simulation of ground motion records by consideration of spectral acceleration correlation, in *Proc. of the 6th International Conference of Seismology and Earthquake Engineering*, Tehran, Iran, 16–18 May 2011.

Sasaki, F., T. Maeda, and Y. Yamamoto (2003). Artificial ground motion with non-stationarity generated using the wavelet analysis, in *Proc. of the 17th Structural Mechanics in Reactor Technology (SMiRT17)*, Prague, Czech Republic, 17–22 August 2003.

Sgobba, S., P. J. Stafford, G. C. Marano, and C. Guaragnella (2011). An evolutionary stochastic ground-motion model defined by a seismological scenario and local site conditions, *Soil Dynam. Earthq. Eng.* **31,** no. 11, 1465–1479.

Shinozuka, M., and G. Deodatis (1988). Stochastic process models for earthquake ground motion, *Prob. Eng. Mech.* **3,** no. 3, 114–123.

Shinozuka, M., and Y. Sato (1967). Simulation of nonstationary random process, *J. Eng. Mech. ASCE* **93,** 11–40.

Spanos, P., A. Giaralis, and N. Politis (2007). Time-frequency representation of earthquake accelerograms and inelastic structural response records using the adaptive chirplet decomposition and empirical mode decomposition, *Soil Dynam. Earthq. Eng.* **27,** no. 7, 675–689.

Spanos, P. D., A. Giaralis, N. P. Politis, and J. M. Roesset (2007). Numerical treatment of seismic accelerograms and of inelastic seismic structural responses using harmonic wavelets, *Computer-Aided Civil Infrastruct. Eng.* **22,** no. 4, 254–264.

Thráinsson, H., and A. S. Kiremidjian (2002). Simulation of digital earthquake accelerograms using the inverse discrete Fourier transform, *Earthq. Eng. Struct. Dyn.* **31,** no. 12, 2023–2048.

Tothong, P., and C. A. Cornell (2007). Probabilistic seismic demand analysis advanced ground motion intensity measures, attenuation relationships, and near-fault effects, *Technical Report Blume Center Report 161*, Stanford, California.

Travasarou, T., J. D. Bray, and N. A. Abrahamson (2003). Empirical attenuation relationship for Arias Intensity, *Earthq. Eng. Struct. Dynam.* **32,** no. 7, 1133–1155.

Trifunac, M. D., and A. G. Brady (1976). A study on the duration of strong earthquake ground motion, *Bull. Seismol. Soc. Am.* **65,** no. 3, 581–626.

Yamamoto, Y., and J. W. Baker (2011). Stochastic model for earthquake ground motion using wavelet packets, *Technical Report Blume Center Report 176*, Stanford, California.

Model Development, Risk Management Solutions
7575 Gateway Blvd.
Newark, California 94560
yyamamoto@rms.com
(Y.Y.)

Department of Civil and Environmental Engineering
Stanford University
Stanford, California 94305
bakerjw@stanford.edu
(J.W.B.)

Manuscript received 12 October 2012;
Published Online 22 October 2013